



1 Ozone pollution in China affected by stratospheric quasi-  
2 biennial oscillation

3  
4  
5

6 Mengyun Li<sup>1</sup>, Yang Yang<sup>1\*</sup>, Hailong Wang<sup>2</sup>, Huimin Li<sup>1</sup>, Pinya Wang<sup>1</sup>, Hong  
7 Liao<sup>1</sup>

8  
9

10 <sup>1</sup>Jiangsu Key Laboratory of Atmospheric Environment Monitoring and  
11 Pollution Control, Jiangsu Collaborative Innovation Center of Atmospheric  
12 Environment and Equipment Technology, School of Environmental Science  
13 and Engineering, Nanjing University of Information Science and Technology,  
14 Nanjing, Jiangsu, China

15 <sup>2</sup>Atmospheric Sciences and Global Change Division, Pacific Northwest  
16 National Laboratory, Richland, Washington, USA

17  
18  
19

20 \*Correspondence to yang.yang@nuist.edu.cn



21 **Abstract**

22 In recent years, near-surface ozone ( $O_3$ ) level has been rising fast in China,  
23 with increasing damages to human health and ecosystems. In this study, the  
24 impact of stratospheric quasi-biennial oscillation (QBO) on interannual  
25 variations in summertime tropospheric  $O_3$  over China is investigated based on  
26 GEOS-Chem model simulations and satellite retrievals. QBO has a significant  
27 positive correlation with near-surface  $O_3$  concentrations over central China  
28 ( $92.5^\circ$ – $112.5^\circ$ E,  $26^\circ$ – $38^\circ$ N) when the sea surface temperature (SST) over the  
29 eastern tropical Pacific is warmer than normal, with a correlation coefficient of  
30 0.53, but QBO has no significant effect on  $O_3$  under the cold SST anomaly.  
31 Compared to the easterly phase of QBO, the near-surface  $O_3$  concentrations  
32 have an increase of up to 3 ppb (5% relative to the average) over central China  
33 during its westerly phase under the warm SST anomaly.  $O_3$  also increases  
34 above the surface and up to the upper troposphere, with a maximum increase  
35 of 2–3 ppb (3–5%) in 850–500 hPa over central China comparing westerly  
36 phase to easterly phase. Process-based analysis and sensitivity simulations  
37 suggest that the  $O_3$  increase over central China is mainly attributed to the  
38 anomalous downward transport of  $O_3$  during the westerly phase of QBO when  
39 a warm SST anomaly occurs in the eastern tropical Pacific, while the local  
40 chemical reactions and horizontal transport processes partly offset the  $O_3$   
41 increase. This work suggests a potentially important role of QBO and the  
42 related vertical transport process in affecting near-surface  $O_3$  air quality, with  
43 an indication for  $O_3$  pollution prediction and prevention.

44

45

46

47

48

49



## 50 **1. Introduction**

51 Ozone (O<sub>3</sub>) is an important atmospheric trace gas. The presence of O<sub>3</sub> in  
52 the stratosphere plays a crucial role in protecting the environment and humans  
53 from UV light, but it is detrimental to human health, ecosystem and agricultural  
54 production within the troposphere (Wang et al., 2007; Nuvolone et al., 2018;  
55 Zhao et al., 2020). Tropospheric O<sub>3</sub> is primarily produced by photochemical  
56 reactions of nitrogen oxides (NO<sub>x</sub>) and volatile organic compounds (VOCs)  
57 (Wang et al., 2017). Apart from precursor emissions, the temporal and spatial  
58 distribution of tropospheric O<sub>3</sub> is highly impacted by meteorological conditions,  
59 among which low relative humidity (RH), cloud free, strong solar radiation and  
60 high temperatures can lead to O<sub>3</sub> pollution by enhancing its chemical production  
61 (Camalier et al., 2007; Porter et al., 2019; Gong and Liao, 2019; Qu et al., 2021;  
62 Wang et al., 2022). The downward transport of stratospheric O<sub>3</sub> into the  
63 troposphere is also one of the sources for near-surface O<sub>3</sub> (Zeng et al., 2010;  
64 Wespes et al., 2017).

65 With the accelerated industrialization and urbanization in recent decades,  
66 the air quality problem has become serious in China (Verstraeten et al., 2015;  
67 Yang et al., 2022). Although many environmental protection and control  
68 measures have been implemented to prevent air pollution (Feng et al., 2019),  
69 O<sub>3</sub> pollution is getting worse in China in the most recent decade (Li et al., 2019;  
70 Gao et al., 2022). Therefore, the factors causing O<sub>3</sub> pollution have been a  
71 research focus in recent years. Many previous studies found that interannual  
72 variations in large-scale circulations modulated the O<sub>3</sub> pollution in China (e.g.,  
73 Yang et al., 2014; Yin et al., 2017; Zhao and Wang, 2017). For example, Yang  
74 et al. (2014) showed that summertime O<sub>3</sub> levels in China were positively  
75 correlated with the strength of East Asian summer monsoon (EASM)  
76 associated with variations in large-scale circulations, which led to an increase  
77 in O<sub>3</sub> concentration exceeding 6% in the strong EASM years relative to the  
78 weak ones.



79 El Niño–Southern Oscillation (ENSO) is the most pronounced mode of  
80 internal variability of the Earth’s climate system, which contains warm (El Niño)  
81 and cold (La Niña) phases, describing anomalous warming and cooling of  
82 surface waters, respectively, in the central-eastern tropical Pacific Ocean. It can  
83 be responsible for global and regional oceanic and atmospheric pattern  
84 anomalies, having significant impacts on wind, temperature and precipitation in  
85 China (Zhou et al., 2007; Xu et al., 2007; Li et al., 2020; Zeng et al., 2021).  
86 Recent studies have shown that the interannual variations in O<sub>3</sub> concentrations  
87 over China are influenced by ENSO events (Jiang and Li, 2022; Li et al., 2022;  
88 Yang et al., 2022). Using the GEOS-Chem model, Yang et al. (2022) showed  
89 that summertime O<sub>3</sub> over southern China had a positive correlation with Niño  
90 3.4 index. Near-surface O<sub>3</sub> concentrations increased by a maximum over 20%  
91 in southern China during El Niño compared to La Niña, which was closely linked  
92 to a weakened southerly over southern China that was conducive to the  
93 accumulation of O<sub>3</sub>. However, they also reported an unusual O<sub>3</sub> changes over  
94 30°–40°N in China that could not be explained by the ENSO impact alone.

95 Quasi-Biennial Oscillation (QBO) is a major mode of variability of zonal  
96 wind in the stratosphere characterized by alternating easterly and westerly, with  
97 a period close to 28 months. The QBO is able to modulate large-scale vertical  
98 and meridional circulations between tropics and subtropics (Punge et al., 2009),  
99 which impacts the East Asian climate. For example, it is reported that southern  
100 China sea summer monsoon is weakened during the QBO westerly phase due  
101 to the associated anomalous Hadley-like circulation (Zheng et al., 2007). Kim  
102 et al. (2020) revealed that there was stronger precipitation over East Asia with  
103 a larger Madden-Julian oscillation (MJO) amplitude when the QBO is in easterly  
104 phase, which is because MJO-induced vertical motion and moisture transport  
105 is amplified by easterly QBO. Therefore, it is of interest to explore the influence  
106 of QBO on interannual variations in summertime O<sub>3</sub> pollution over China and  
107 their connections during anomalous modes of sea surface temperature (SST)



108 over the eastern tropical Pacific, as well as the mechanisms involved.

109 In the present study, the impact of QBO on O<sub>3</sub> variations in China is  
110 examined based on GEOS-Chem simulations over 1981–2020, together with  
111 satellite retrievals. The paper is organized as follows: In Section 2, we describe  
112 the model, numerical experiments, the reanalysis datasets, the indices used in  
113 this study and satellite retrieval data. The connection between QBO and  
114 tropospheric O<sub>3</sub> in China and the possible mechanisms are explored in Section  
115 3. Conclusions and discussion are given in Section 4.

## 116 **2. Methods**

### 117 **2.1. GEOS-Chem model simulations**

118 GEOS-Chem is a global three-dimensional chemical transport model with  
119 comprehensive chemistry mechanisms of O<sub>3</sub>-NO<sub>x</sub>-hydrocarbon-aerosol  
120 involved in the model (Zhai et al., 2021). In this study, we apply the GEOS-  
121 Chem version 12.9.3 to simulate O<sub>3</sub> from 1981 to 2020. The horizontal grid of  
122 the model is 2° × 2.5° (latitude × longitude) with 47 vertical levels above the  
123 surface. Stratospheric O<sub>3</sub> is calculated based on the linearized chemistry  
124 mechanism (McLinden et al., 2000). Meteorological fields driving the GEOS-  
125 Chem simulations are from the Modern-Era Retrospective analysis for  
126 Research and Applications version 2 (MERRA-2) (Gelaro et al., 2017),  
127 produced by the NASA's Global Modeling and Assimilation Office.

128 Anthropogenic emissions in China are obtained from the Multi-resolution  
129 Emission Inventory for China (MEIC) (Zheng et al., 2018). Anthropogenic  
130 emissions outside China are adopted from the Community Emissions Data  
131 System (CEDS) version 20210205 (Hoesly et al., 2018). Biogenic emissions  
132 employ the Model of Emissions of Gases and Aerosols from Nature (MEGAN)  
133 version 2.1 (Guenther et al., 2012). Global biomass burning emissions are from  
134 the Global Fire Emissions Database version 4 (GFED4) (van der Werf et al.,  
135 2017). Soil NO<sub>x</sub> emissions are estimated in a soil parameterization scheme  
136 (Hudman et al., 2012). Lightning-produced NO<sub>x</sub> emissions are estimated in the



137 model based on Murray et al. (2012) and Ott et al. (2010).

138 The GEOS-Chem simulations are performed to assess the impact of QBO  
139 on interannual variation of O<sub>3</sub> covering the period of 1981–2020, following a 6-  
140 month model spin-up. In order to minimize the impact of interannual variations  
141 in emissions on the modeled O<sub>3</sub> concentrations, the anthropogenic, biogenic  
142 burning and natural emissions of O<sub>3</sub> precursors are all fixed at their 2017 levels  
143 in the base simulation (BASE). The BASE simulation is analyzed to quantify the  
144 impact of QBO on O<sub>3</sub>, unless stated otherwise.

145 A sensitivity simulation (NO\_CHN) is conducted with a different emission  
146 configuration than BASE, aiming to investigate the impact of domestic  
147 emissions in China on tropospheric O<sub>3</sub> during QBO events. Different from BASE,  
148 anthropogenic emissions of NO<sub>x</sub>, CO and VOCs in China are turned off in  
149 NO\_CHN. Considering that O<sub>3</sub> pollution is most critical during the boreal  
150 summer, only summer months (June-July-August, JJA) are examined in this  
151 study. Time-varying meteorological fields follow those from MERRA-2 during all  
152 simulations.

153 Figure 1 compares the year-by-year changes in JJA O<sub>3</sub> concentrations in  
154 observations and BASE simulation. GEOS-Chem can roughly capture the  
155 interannual variation in surface O<sub>3</sub> concentrations in China during 2016–2020.  
156 The spatial correlation coefficients between the observed and modeled year-  
157 by-year changes in O<sub>3</sub> concentrations are about 0.5–0.6, except the 2018-to-  
158 2019 changes in O<sub>3</sub>, which can be attributed to the strong influence of  
159 emissions on observed O<sub>3</sub> concentrations.

## 160 **2.2. QBO and Niño 3.4 indices**

161 The QBO phases are determined by the zonal average of 30 hPa zonal  
162 wind over the equator (5°S–5°N) based on MERRA-2 reanalysis (Fig. 2a).  
163 Positive values denote westerly QBO phase (QBOW), while negative values  
164 denote easterly QBO phase (QBOE).

165 Niño 3.4 index is used to characterize the warm and cold phases of SST



166 anomaly over the eastern tropical Pacific, which is estimated as the SST  
167 anomalies over the Niño 3.4 region ( $5^{\circ}\text{S}$ – $5^{\circ}\text{N}$ ,  $170^{\circ}$ – $120^{\circ}\text{W}$ ) (Fig. 2b). Positive  
168 (negative) Niño 3.4 index indicates a warm (cold) phase when SST in eastern  
169 tropical Pacific is higher (lower) than the climatological mean (1981–2020). The  
170 40 years can be divided into the warm and cold phases of the JJA SST  
171 anomalies over the eastern tropical Pacific according to Niño 3.4 index.

172 QBO and Niño 3.4 indices calculated in this study using MERRA-2  
173 reanalysis are highly correlated with those derived from HadISST1 and  
174 NCEP/NCAR reanalysis, with correlation coefficients of 0.98 and 0.97,  
175 respectively. It suggests that the QBO and the eastern tropical Pacific SST  
176 anomaly are well represented in the GEOS-Chem simulations, which is  
177 important for appropriately quantifying impacts of QBO on the interannual  
178 variations in  $\text{O}_3$  variations over China.

### 179 **2.3 Satellite data**

180 The monthly mean tropospheric column  $\text{O}_3$  (TCO) data from Ozone  
181 Monitoring Instrument/Microwave Limb Sounder (OMI/MLS) on board the Aura  
182 satellite since 2004 are used to verify the modeled impact of QBO on  $\text{O}_3$   
183 pollution in China. The grid resolution of OMI/MLS data is  $1.25^{\circ}$  longitude  $\times$   $1.0^{\circ}$   
184 latitude, covering the measurement area between  $60^{\circ}\text{S}$  and  $60^{\circ}\text{N}$ . TCO is  
185 calculated by subtracting MLS stratospheric column  $\text{O}_3$  from OMI total column  
186  $\text{O}_3$  (Ziemke et al., 2011). The tropopause height is calculated according to  $2\text{ K}$   
187  $\text{km}^{-1}$  lapse rate, which generally locates around 150 hPa in mid-latitudes (Jing  
188 et al., 2006; Peiro et al., 2018). In this study, we used 150 hPa as an  
189 approximation of the tropopause level for the calculation of TCO from the model  
190 simulation, although it may lead to a small bias in the magnitude of TCO.

## 191 **3. Result**

### 192 **3.1. Impact of QBO on tropospheric $\text{O}_3$ in China**

193 To illustrate the effects of QBO on summertime near-surface  $\text{O}_3$  over China,  
194 the spatial distribution of the correlation coefficients between the JJA  $\text{O}_3$



195 concentrations and concurrent QBO index is presented in Fig. 3a. It shows that  
196 the correlation coefficients between QBO index and surface O<sub>3</sub> are insignificant  
197 over most regions of China, except for part of Qinghai province, which means  
198 that the single impact of QBO events cannot significantly affect O<sub>3</sub> pollution in  
199 China. Previous studies have shown that the impact of QBO can be  
200 compounded with ENSO (Sun et al., 2019; Xue et al., 2015). Motivated by these  
201 studies, we further examine the relationships between QBO and summertime  
202 O<sub>3</sub> in the warm/cold phases of SST anomalies of the eastern tropical Pacific.  
203 Note that the correlation coefficient between QBO index and Niño 3.4 index is  
204 only 0.09, indicating that there is no direct linear relationship between QBO and  
205 ENSO, which has also been reported in previous studies (Christiansen et al.,  
206 2016; Sun et al., 2019).

207 The influences of QBO on O<sub>3</sub> under different SST anomalies over the  
208 eastern tropical Pacific are quite different (Fig. 3b and 3c). During years under  
209 the warm SST phase, significant correlations between JJA near-surface O<sub>3</sub>  
210 concentrations and QBO index are located over the latitudinal band of 25°–  
211 40°N in China. In central China (92.5°–112.5°E, 26°–38°N), the correlation  
212 coefficient between the regionally averaged O<sub>3</sub> concentration and QBO index  
213 under the warm phase is 0.53, which is much higher than 0.23 during the whole  
214 40-year period. However, under the cold ENSO phase, there is no significant  
215 correlation over China, with a regional correlation coefficient of –0.06. These  
216 results suggest that QBO may have a remarkable effect on tropospheric O<sub>3</sub>  
217 over central China during the warm anomaly of the eastern tropical Pacific SST,  
218 while it has little impact on O<sub>3</sub> in China during years with cold SST anomalies.  
219 Once there is a coincidence of QBOW and warm SST anomaly in eastern  
220 tropical Pacific, the combined effects could worsen the O<sub>3</sub> pollution over China.  
221 Therefore, the three strongest QBOW (1990, 1997 and 2019) and QBOE (1994,  
222 2012 and 2018) years under the warm phase of SST anomaly during the past  
223 four decades are chosen to further quantify the influence of QBO on O<sub>3</sub> pollution





224 in China.

225 Figure 4 presents JJA O<sub>3</sub> anomalies in the selected QBOW and QBOE  
226 years relative to the climatological mean (1981–2020). Under the combined  
227 influence of QBOW and warm SST anomaly, positive O<sub>3</sub> concentration  
228 anomalies are observed over central and southern China. In contrast, the  
229 surface O<sub>3</sub> concentration increases over southern China while it decreases in  
230 central China during QBOE years. The increases in O<sub>3</sub> levels over southern  
231 China under warm SST anomaly in both QBOW and QBOE years are due to  
232 the positive correlation between Niño 3.4 index and tropospheric O<sub>3</sub>  
233 concentrations in southern China. Previous studies have reported that O<sub>3</sub>  
234 concentrations increased over southern China during El Niño years, which is  
235 related to O<sub>3</sub> convergence due to weakened southerlies (Yang et al., 2022; Li  
236 et al., 2022). The different characteristics of O<sub>3</sub> changes in central China  
237 highlight the role of QBO in affecting the distribution of O<sub>3</sub> over China under  
238 warm SST anomalies of the eastern tropical Pacific.

239 Figure 5 presents the spatial distribution near the surface and pressure–  
240 longitude cross-sections of absolute and percentage differences between  
241 QBOW and QBOE in O<sub>3</sub> concentrations over China under the warm SST  
242 anomaly. Compared with QBOE years, positive O<sub>3</sub> concentration anomalies are  
243 located between 25°N and 40°N over China during QBOW, especially over  
244 central China where the maximum anomaly exceeds 3 ppb (parts per billion)  
245 (or 5% relative to the climatological average). The simulated O<sub>3</sub> pollution  
246 enhancement is also shown in the vertical distribution of the zonal mean (26°–  
247 38°N) composite differences (Fig. 5b, d). For QBOW years, increased O<sub>3</sub>  
248 occurred in the whole troposphere, with the maximum increase of 2–3 ppb (3–  
249 5%) between 850 hPa and 500 hPa over central China, indicating a high  
250 probability of enhanced O<sub>3</sub> pollution during QBOW relative to QBOE. O<sub>3</sub>  
251 concentrations also increase in the coastal area of eastern China, which is  
252 mainly due to the decreases in O<sub>3</sub> concentrations in the selected QBOE years



253 relative to the climatological mean, as the O<sub>3</sub> concentrations only slightly  
254 increase in the QBOW years. The correlation between O<sub>3</sub> and QBO index over  
255 this region is not as strong as that over central China, which indicates that the  
256 anomalous increase in O<sub>3</sub> over the coastal area of eastern China may not be a  
257 typical feature of the QBO impact and will not be discussed hereafter.

258 The modeled difference in summertime tropospheric O<sub>3</sub> between the  
259 QBOW and QBOE years can also be observed from satellite (Fig. 6). The  
260 OMI/MLS retrieved TCO are higher in QBOW than QBOE years between 25°–  
261 35°N in China, which is in accordance with the model results. Averaged over  
262 central China, the difference in TCO between the selected QBOW (2019) and  
263 QBOE years (2012 and 2018) from satellite data is 2.8 DU, similar to the 2.5  
264 DU from model simulation. Both model simulations and satellite retrievals  
265 suggest that the QBO can significantly influence tropospheric O<sub>3</sub> in China.

### 266 **3.2. Mechanism of the QBO impacts on O<sub>3</sub> in China**

267 Composite differences of relevant meteorological variables between the  
268 selected QBOW and QBOE years are shown in Fig. 7 to illustrate mechanisms  
269 of the QBO impacts on O<sub>3</sub> in China. During QBOW years under warm SST  
270 anomaly, the decrease in cloud fraction (Fig. 7g) allows more solar radiation to  
271 reach the surface (Fig. 7h) and the RH also decreases over central China (Fig.  
272 7e), relative to QBOE years. These changes in meteorological parameters tend  
273 to increase the photochemical production of O<sub>3</sub>. However, the air temperature  
274 significantly decreases in the lower (Fig. 7i) and mid-troposphere (Fig. 7f) in  
275 QBOW years compared to QBOE years, which suppresses the O<sub>3</sub> production.  
276 The combined effect of the changes in these meteorological parameters leads  
277 to a reduction in net O<sub>3</sub> chemical production by about 1% over central China in  
278 QBOW compared to QBOE years based on an integrated process rate analysis  
279 (Lou et al., 2015; Qu et al., 2021; Zhu et al., 2021). Therefore, the chemical  
280 production change is not the major process causing the O<sub>3</sub> pollution  
281 deterioration during QBOW years under the warm SST anomaly.



282 Compared with QBOE years, anomalous northwesterly winds at 850 hPa  
283 occurred over central China during the QBOW years, located at the east edge  
284 of an anomalous high over western China (Fig. 7a). Under the influence of this  
285 anomalous high, the anomalous downdraft over central China (Fig. 7c) can  
286 reduce the vertical transport of O<sub>3</sub> to the upper troposphere, which leads to an  
287 O<sub>3</sub> accumulation in the lower and mid-troposphere. In addition, the increase in  
288 planetary boundary layer height (Fig. 7d) also favors the vertical O<sub>3</sub> mixing  
289 between the lower and upper troposphere in QBOW relative to QBOE years.

290 Considering the effect of winds on O<sub>3</sub> transport, the horizontal JJA O<sub>3</sub> mass  
291 fluxes from the surface to 850 hPa and the vertical mass flux at 850 hPa over  
292 central China are calculated and summarized in Table 1. Due to an anomalous  
293 northwesterly, the outflow transport of O<sub>3</sub> from the north boundary of central  
294 China is reduced by 1.11 Tg during QBOW years relative to QBOE years.  
295 However, through the east boundary of central China, an inflow transport of O<sub>3</sub>  
296 is reduced by 1.35 Tg, which overwhelms the gain from the reduced northward  
297 transport. The O<sub>3</sub> flux changes through the west and south boundaries are  
298 relatively small and almost offset each other. The overall changes in the  
299 horizontal transport result in a decrease in O<sub>3</sub> mass by 0.29 Tg from surface to  
300 850 hPa in QBOW relative to QBOE years, suggesting that the horizontal  
301 advection change is also not the primary process causing the enhanced O<sub>3</sub>  
302 pollution.

303 The anomalous downdraft over central China weakens the upward mixing  
304 of high lower-tropospheric O<sub>3</sub> concentrations and causes an anomalous  
305 downward transport of O<sub>3</sub> by 0.59 Tg at 850 hPa, contributing to the increase  
306 in surface O<sub>3</sub> concentrations. Therefore, the impact of the QBO under warm  
307 SST anomaly on the distribution of tropospheric O<sub>3</sub> over central China is mainly  
308 via changes in the vertical motion.

### 309 **3.3. Role of China domestic anthropogenic emission**

310 Comparison of the O<sub>3</sub> anomaly in BASE and NO\_CHN identifies the impact



311 of China domestic emissions on O<sub>3</sub> concentrations. When domestic  
312 anthropogenic emissions of O<sub>3</sub> precursors are turned off, JJA mean near-  
313 surface O<sub>3</sub> concentrations largely increase across China, especially between  
314 30°–40°N, with maximum increases exceeding 5 ppb during QBOW compared  
315 to QBOE years (Fig. 8a). Averaged over central China, the anomalous increase  
316 in near-surface O<sub>3</sub> concentration is 3.0 ppb in NO\_CHN, even higher than that  
317 (1.7 ppb) in BASE simulation. It is consistent with the finding that the vertical  
318 transport plays a dominant role in enhancing the surface O<sub>3</sub> levels over central  
319 China during QBOW years, even though the reduced O<sub>3</sub> photochemical  
320 production, primarily determined by the domestic emissions, weakens the O<sub>3</sub>  
321 pollution in QBOW relative to QBOE years in BASE simulation.

322 Figure 8b shows the simulated vertical distribution of O<sub>3</sub> concentration  
323 difference between the selected QBOW and QBOE years from the NO\_CHN  
324 experiment. The positive O<sub>3</sub> anomaly in the troposphere is similar to that from  
325 the BASE experiment, but the increases are mainly between 95°E and 115°E  
326 from the surface to 500 hPa over central China. These results suggest that the  
327 vertical transport process dominates the increase in summertime tropospheric  
328 O<sub>3</sub> concentrations over central China during QBOW under warm SST anomaly  
329 of the eastern tropical Pacific. The reduced photochemical production of O<sub>3</sub>  
330 from China domestic anthropogenic emissions is not as important as changes  
331 in the vertical transport in inducing O<sub>3</sub> pollution in QBOW compared to QBOE  
332 years.

#### 333 **4. Conclusion and discussion**

334 Based on GEOS-Chem model simulations over 1981–2020, we  
335 investigate the impacts of different QBO events on the surface and tropospheric  
336 O<sub>3</sub> over China. Although only weak correlations are found between JJA mean  
337 near-surface O<sub>3</sub> concentrations and QBO index over China, their positive  
338 correlation is significant in years with warm SST anomalies over the eastern  
339 tropical Pacific. Averaged over central China (92.5°–112.5°E, 26°–38°N), the



340 correlation coefficient between the regional near-surface O<sub>3</sub> concentration and  
341 QBO index during the warm ENSO phase is 0.53. It suggests that the co-  
342 occurrence of the westerly phase of QBO and warm SST anomalies over the  
343 eastern tropical Pacific would exacerbate summertime O<sub>3</sub> pollution in China.  
344 Compared with QBOE years, near-surface O<sub>3</sub> concentrations increase by up to  
345 3 ppb (5% relative to the average) across China during QBOW, especially over  
346 central China, and the increase in O<sub>3</sub> extends from the surface to the upper  
347 troposphere, especially between 850 hPa and 500 hPa.

348 A combined effect of changes in meteorological conditions (i.e., less cloud,  
349 higher RH, and lower temperature) leads to a slightly lower net O<sub>3</sub> chemical  
350 production rate in QBOW years than in QBOE years. Central China is  
351 influenced by anomalous northwesterlies during QBOW, which weakens O<sub>3</sub>  
352 import from the east boundary and the export from north boundary of central  
353 China, leading to a net O<sub>3</sub> export of 0.29 Tg during QBOW, compared to QBOE  
354 years, from surface to 850 hPa. However, change in the vertical transport is the  
355 main process causing O<sub>3</sub> concentration increases in QBOW years. An  
356 anomalous downdraft leads to the O<sub>3</sub> mass increase of 0.59 Tg below 850 hPa  
357 by suppressing vertical mixing and promoting O<sub>3</sub> accumulation in the lower  
358 troposphere. The sensitivity experiment with China domestic anthropogenic  
359 emissions of O<sub>3</sub> precursors turned off shows a greater increase of O<sub>3</sub> (3.0 ppb)  
360 than that in the default simulation (1.7 ppb). It indicates that the O<sub>3</sub> increase  
361 over central China during QBOW years under the warm SST anomaly is mainly  
362 due to the anomalous vertical transport, while a decrease in local chemical  
363 production partly offsets the O<sub>3</sub> increases in central China. Moreover, the  
364 positive anomaly of TCO based on GEOS-Chem model simulation is consistent  
365 with the satellite retrieval from the OMI/MLS.

366 This study explores the effect of QBO on tropospheric O<sub>3</sub> over China and  
367 the underlying mechanisms during the warm SST anomalies of the eastern  
368 tropical Pacific, which can improve the understanding of causes of O<sub>3</sub> pollution



369 over China. For climatological average, prevailing easterly winds at 30 hPa  
370 dominate the equator, accompanied by the upward motion over central China  
371 within the troposphere. During QBOW years, the prevailing winds reverse to  
372 westerlies, which may induce the anomalous downward motion over central  
373 China. However, the dynamical mechanism of how the stratospheric QBO  
374 drives changes in the vertical motion and circulation patterns in China along  
375 with the SST anomaly over the eastern tropical Pacific is out of the scope of  
376 this study and merits further investigation. Nevertheless, the QBO index is  
377 positively correlated with the vertical velocity throughout the troposphere over  
378 China, especially between 100°E and 110°E (Fig. 9), where the lower  
379 tropospheric O<sub>3</sub> increases the most in the NO\_CHN experiment during QBOW  
380 years under the warm SST anomaly. These positive correlations demonstrate  
381 that the weakened (strengthened) upward motion increase (decrease)  
382 tropospheric O<sub>3</sub> concentrations during QBOW (QBOE) years, confirming that  
383 changes in the vertical transport driven by QBO events play an important role  
384 in modulating summertime O<sub>3</sub> pollution over China. The phenomenon of  
385 changes in tropospheric O<sub>3</sub> between different QBO phases is also verified by  
386 satellite retrievals.  
387



388 **Author contributions.** YY designed the research; ML performed simulations  
389 and analyzed the data. All authors including HW, LH, PW, and HL discussed  
390 the results and wrote the paper.

391

392 **Code and data availability.** The GEOS-Chem model is available at  
393 <https://zenodo.org/record/3974569#.YTD81NMzagR> (last access: 1 July 2022).  
394 MERRA-2 reanalysis data can be downloaded at  
395 <https://gmao.gsfc.nasa.gov/reanalysis/MERRA-2/> (last access: 1 July 2022).  
396 The monthly mean tropospheric O<sub>3</sub> data from OMI/MLS is downloaded from  
397 [https://acd-ext.gsfc.nasa.gov/Data\\_services/cloud\\_slice/new\\_data.html](https://acd-ext.gsfc.nasa.gov/Data_services/cloud_slice/new_data.html) (last  
398 access: 1 July 2022). Our model results are available at  
399 <https://doi.org/10.5281/zenodo.6793180>. O<sub>3</sub> observations are obtained from  
400 China National Environmental Monitoring Centre (CNEMC,  
401 <http://www.cnemc.cn/en/>).

402

403 **Acknowledgments.** HW acknowledges the support by the U.S. Department of  
404 Energy (DOE), Office of Science, Office of Biological and Environmental  
405 Research (BER), as part of the Earth and Environmental System Modeling  
406 program. The Pacific Northwest National Laboratory (PNNL) is operated for  
407 DOE by the Battelle Memorial Institute under contract DE-AC05-76RLO1830.

408

409 **Financial support.** This study was supported by the National Natural Science  
410 Foundation of China (grant 41975159) the National Key Research and  
411 Development Program of China (grant 2020YFA0607803 and  
412 2019YFA0606800) and Jiangsu Science Fund for Distinguished Young  
413 Scholars (grant BK20211541).

414

415 **Competing interests.** The authors declare that they have no conflict of interest.



416 **References**

417

418 Camalier, L., Cox, W. M., and Dolwick, P.: The effects of meteorology on  
419 ozone in urban areas and their use in assessing ozone trends, *Atmos.*  
420 *Environ.*, 41, 7127–7137, <https://doi.org/10.1016/j.atmosenv.2007.04.061>,  
421 2007.

422

423 Christiansen, B., Yang, S., and Madsen, M. S.: Do strong warm ENSO events  
424 control the phase of the stratospheric QBO?, *Geophys. Res. Lett.*, 43, 10,489-  
425 10,495, <https://doi.org/10.1002/2016gl070751>, 2016.

426

427 Feng, Y., Ning, M., Lei, Y., Sun, Y., Liu, W., and Wang, J.: Defending blue sky  
428 in China: Effectiveness of the “Air Pollution Prevention and Control Action  
429 Plan” on air quality improvements from 2013 to 2017., *J. Environ. Manage.*,  
430 252, 109603–109603, <https://doi.org/10.1016/j.jenvman.2019.109603>, 2019.

431

432 Gao, J., Yang, Y., Wang, H., Wang, P., Li, H., Li, M., Ren, L., Yue, X., and  
433 Liao, H.: Fast climate responses to emission reductions in aerosol and ozone  
434 precursors in China during 2013–2017, *Atmos. Chem. Phys.*, 22, 7131–7142,  
435 <https://doi.org/10.5194/acp-22-7131-2022>, 2022.

436

437 Gelaro, R., McCarty, W., Suárez, M. J., Todling, R., Molod, A., Takacs, L.,  
438 Randles, C. A., Darmenov, A., Bosilovich, M. G., Reichle, R., Wargan, K., Coy,  
439 L., Cullather, R., Draper, C., Akella, S., Buchard, V., Conaty, A., da Silva, A.  
440 M., Gu, W., Kim, G.-K., Koster, R., Lucchesi, R., Merkova, D., Nielsen, J. E.,  
441 Partyka, G., Pawson, S., Putman, W., Rienecker, M., Schubert, S. D.,  
442 Sienkiewicz, M., and Zhao, B.: The Modern-Era Retrospective Analysis for  
443 Research and Applications, Version 2 (MERRA-2), *J. Climate*, 30, 5419–5454,  
444 <https://doi.org/10.1175/JCLI-D-16-0758.1>, 2017.

445

446 Gong, C. and Liao, H.: A typical weather pattern for ozone pollution events in  
447 North China, *Atmos. Chem. Phys.*, 19, 13725–13740,  
448 <https://doi.org/10.5194/acp-19-13725-2019>, 2019.

449

450 Guenther, A. B., Jiang, X., Heald, C. L., Sakulyanontvittaya, T., Duhl, T.,  
451 Emmons, L. K., and Wang, X.: The Model of Emissions of Gases and  
452 Aerosols from Nature version 2.1 (MEGAN2.1): an extended and updated  
453 framework for modeling biogenic emissions, *Geosci. Model Dev.*, 5, 1471–  
454 1492, <https://doi.org/10.5194/gmd-5-1471-2012>, 2012.

455

456 Hoesly, R. M., Smith, S. J., Feng, L., Klimont, Z., Janssens-Maenhout, G.,  
457 Pitkanen, T., Seibert, J. J., Vu, L., Andres, R. J., Bolt, R. M., Bond, T. C.,  
458 Dawidowski, L., Kholod, N., Kurokawa, J., Li, M., Liu, L., Lu, Z., Moura, M. C.  
459 P., O'Rourke, P. R., and Zhang, Q.: Historical (1750–2014) anthropogenic





- 460 emissions of reactive gases and aerosols from the Community Emissions  
461 Data System (CEDS), *Geosci. Model Dev.*, 11, 369–408,  
462 <https://doi.org/10.5194/gmd-11-369-2018>, 2018.  
463  
464 Hudman, R. C., Moore, N. E., Mebust, A. K., Martin, R. V., Russell, A. R.,  
465 Valin, L. C., and Cohen, R. C.: Steps towards a mechanistic model of global  
466 soil nitric oxide emissions: implementation and space based-constraints,  
467 *Atmos. Chem. Phys.*, 12, 7779–7795, [https://doi.org/10.5194/acp-12-7779-](https://doi.org/10.5194/acp-12-7779-2012)  
468 2012, 2012.  
469  
470 Jiang, Z. and Li, J.: Impact of eastern and central Pacific El Niño on lower  
471 tropospheric ozone in China, *Atmos. Chem. Phys.*, 22, 7273–7285,  
472 <https://doi.org/10.5194/acp-22-7273-2022>, 2022.  
473  
474 Jing, P., Cunnold, D., Choi, Y., and Wang, Y.: Summertime tropospheric ozone  
475 columns from Aura OMI/MLS measurements versus regional model results  
476 over the United States, *Geophys. Res. Lett.*, 33, L17817,  
477 <https://doi.org/10.1029/2006GL026473>, 2006  
478  
479 Kim, H., Son, S.W., and Yoo, C.: QBO modulation of the MJO-related  
480 precipitation in East Asia, *J. Geophys. Res.*, 125, e2019JD031929,  
481 <https://doi.org/10.1029/2019JD031929>, 2020.  
482  
483 Li, H., Fan, K., He, S., Liu, Y., Yuan, X., and Wang, H.: Intensified Impacts of  
484 Central Pacific ENSO on the Reversal of December and January Surface Air  
485 Temperature Anomaly over China since 1997, *J. Clim.*, 34, 1601–1618,  
486 <https://doi.org/10.1175/jcli-d-20-0048.1>, 2020.  
487  
488 Li, K., Jacob, D. J., Liao, H., Shen, L., Zhang, Q., and Bates, K.:  
489 Anthropogenic drivers of 2013–2017 trends in summer surface ozone in  
490 China, 116, 422–427, <https://doi.org/10.1073/pnas.1812168116>, 2019.  
491  
492 Li, M., Yang, Y., Wang, P., Ji, D., and Liao, H.: Impacts of strong El Niño on  
493 summertime near-surface ozone over China, *Atmos. Ocean. Sci. Lett.*,  
494 100193, <https://doi.org/10.1016/j.aosl.2022.100193>, 2022.  
495  
496 Lou, S., Liao, H., Yang, Y., and Mu, Q.: Simulation of the interannual  
497 variations of tropospheric ozone over China: Roles of variations in  
498 meteorological parameters and anthropogenic emissions, *Atmos. Environ.*,  
499 122, 839–851, <https://doi.org/10.1016/j.atmosenv.2015.08.081>, 2015.  
500  
501 McLinden, C. A., Olsen, S. C., Hannegan, B., Wild, O., Prather, M. J., and  
502 Sundet, J.: Stratospheric ozone in 3-D models: A simple chemistry and the



- 503 cross-tropopause flux, *J. Geophys. Res.*, 105, 14653–14665,  
504 <https://doi.org/10.1029/2000JD900124>, 2000.  
505  
506 Murray, L. T., Jacob, D. J., Logan, J. A., Hudman, R. C., and Koshak, W. J.:  
507 Optimized regional and interannual variability of lightning in a global chemical  
508 transport model constrained by LIS/OTD satellite data, *J. Geophys. Res.*, 117,  
509 <https://doi.org/10.1029/2012JD017934>, 2012.  
510  
511 Nuvolone, D., Petri, D., and Voller, F.: The effects of ozone on human health,  
512 *Environ. Sci. Pollut. R.*, 25, 8074–8088, [https://doi.org/10.1007/s11356-017-](https://doi.org/10.1007/s11356-017-9239-3)  
513 [9239-3](https://doi.org/10.1007/s11356-017-9239-3), 2018.  
514  
515 Ott, L. E., Pickering, K. E., Stenchikov, G. L., Allen, D. J., DeCaria, A. J.,  
516 Ridley, B., Lin, R.-F., Lang, S., and Tao, W. K.: Production of lightning NO<sub>x</sub>  
517 and its vertical distribution calculated from three-dimensional cloud-scale  
518 chemical transport model simulations, *J. Geophys. Res.*, 115, D04301,  
519 <https://doi.org/10.1029/2009JD011880>, 2010.  
520  
521 Peiro, H., Emili, E., Cariolle, D., Barret, B., and Le Flochmoën, E.: Multi-year  
522 assimilation of IASI and MLS ozone retrievals: variability of tropospheric  
523 ozone over the tropics in response to ENSO, *Atmos. Chem. Phys.*, 18, 6939–  
524 6958, <https://doi.org/10.5194/acp-18-6939-2018>, 2018.  
525  
526 Porter, W. C. and Heald, C. L.: The mechanisms and meteorological drivers of  
527 the summertime ozone–temperature relationship, *Atmos. Chem. Phys.*, 19,  
528 13367–13381, <https://doi.org/10.5194/acp-19-13367-2019>, 2019.  
529  
530 Punge, H. J., Konopka, P., Giorgetta, M. A., and Müller, R.: Effects of the  
531 quasi-biennial oscillation on low-latitude transport in the stratosphere derived  
532 from trajectory calculations, *J. Geophys. Res.*, 114, D03102,  
533 <https://doi.org/10.1029/2008JD010518>, 2009.  
534  
535 Qu, K., Wang, X., Yan, Y., Shen, J., Xiao, T., Dong, H., Zeng, L., and Zhang,  
536 Y.: A comparative study to reveal the influence of typhoons on the transport,  
537 production and accumulation of O<sub>3</sub> in the Pearl River Delta, China, *Atmos.*  
538 *Chem. Phys.*, 21, 11593–11612, <https://doi.org/10.5194/acp-21-11593-2021>,  
539 2021.  
540  
541 Sun, L., Wang, H., and Liu, F.: Combined effect of the QBO and ENSO on the  
542 MJO, *Atmos. Ocean. Sci. Lett.*, 12, 170–176,  
543 <https://doi.org/10.1080/16742834.2019.1588064>, 2019.  
544  
545 van der Werf, G. R., Randerson, J. T., Giglio, L., van Leeuwen, T. T., Chen, Y.,  
546 Rogers, B. M., Mu, M., van Marle, M. J. E., Morton, D. C., Collatz, G. J.,



- 547 Yokelson, R. J., and Kasibhatla, P. S.: Global fire emissions estimates during  
548 1997–2016, *Earth Syst. Sci. Data*, 9, 697–720, [https://doi.org/10.5194/essd-9-](https://doi.org/10.5194/essd-9-697-2017)  
549 [697-2017](https://doi.org/10.5194/essd-9-697-2017), 2017.
- 550
- 551 Verstraeten, W. W., Neu, J. L., Williams, J. E., Bowman, K. W., Worden, J. R.,  
552 and Boersma, K. F.: Rapid increases in tropospheric ozone production and ex  
553 port from China, *Nat. Geosci.*, 8, 690–695, <https://doi.org/10.1038/ngeo2493>,  
554 2015.
- 555
- 556 Wang, P., Yang, Y., Li, H., Chen, L., Dang, R., Xue, D., Li, B., Tang, J., Leung,  
557 L. R., and Liao, H.: North China Plain as a hot spot of ozone pollution  
558 exacerbated by extreme high temperatures, *Atmos. Chem. Phys.*, 22, 4705–  
559 4719, <https://doi.org/10.5194/acp-22-4705-2022>, 2022.
- 560
- 561 Wang, T., Xue, L., Brimblecombe, P., Lam, Y. F., Li, L., and Zhang, L.: Ozone  
562 pollution in China: A review of concentrations, meteorological influences,  
563 chemical precursors, and effects, *Sci. Total Environ.*, 575, 1582–1596,  
564 <https://doi.org/10.1016/j.scitotenv.2016.10.081>, 2017.
- 565
- 566 Wang, X., Manning, W. J., Feng, Z., and Zhu, Y.-G.: Ground-level ozone in  
567 China: Distribution and effects on crop yields, *Environ. Pollut.*, 147, 394–400,  
568 <https://doi.org/10.1016/j.envpol.2006.05.006>, 2007.
- 569
- 570 Wespes, C., Hurtmans, D., Clerbaux, C., and Coheur, P.-F.: O<sub>3</sub> variability in  
571 the troposphere as observed by IASI over 2008–2016: Contribution of  
572 atmospheric chemistry and dynamics, *J. Geophys. Res. Atmos.*, 122, 2429–  
573 2451, <https://doi.org/10.1002/2016jd025875>, 2017.
- 574
- 575 Xu, Z. X., Li, J. Y., Takeuchi, K., and Ishidaira, H.: Long-term trend of  
576 precipitation in China and its association with the El Niño–southern oscillation,  
577 *Hydrol. Process.*, 21, 61–71, <https://doi.org/10.1002/hyp.6180>, 2007.
- 578
- 579 Xue, X., Chen, W., Chen, S., and Zhou, D.: Modulation of the connection  
580 between boreal winter ENSO and the South Asian high in the following  
581 summer by the stratospheric quasi-biennial oscillation, *J. Geophys. Res.*  
582 *Atmos.*, 120, 7393–7411, <https://doi.org/10.1002/2015JD023260>, 2015.
- 583
- 584 Yang, Y., Ren, L., Wu, M., Wang, H., Song, F., Leung, L. R., Hao, X., Li, J.,  
585 Chen, L., Li, H., Zeng, L., Zhou, Y., Wang, P., Liao, H., Wang, J., and Zhou,  
586 Z.-Q.: Abrupt emissions reductions during COVID-19 contributed to record  
587 summer rainfall in China, *Nat. Commun.*, 13, 959,  
588 <https://doi.org/10.1038/s41467-022-28537-9>, 2022.
- 589



- 590 Yang, Y., Li, M., Wang, H., Li, H., Wang, P., Li, K., Gao, M., and Liao, H.:  
591 ENSO modulation of summertime tropospheric ozone over China, *Environ.*  
592 *Res. Lett.*, 17, 034020, <https://doi.org/10.1088/1748-9326/ac54cd>, 2022.  
593
- 594 Yang, Y., Liao, H., and Li, J.: Impacts of the East Asian summer monsoon on  
595 interannual variations of summertime surface-layer ozone concentrations over  
596 China, *Atmos. Chem. Phys.*, 14, 6867–6879, [https://doi.org/10.5194/acp-14-](https://doi.org/10.5194/acp-14-6867-2014)  
597 [6867-2014](https://doi.org/10.5194/acp-14-6867-2014), 2014.  
598
- 599 Yin, P., Chen, R., Wang, L., Meng, X., Liu, C., Niu, Y., Lin, Z., Liu, Y., Liu, J.,  
600 Qi, J., You, J., Zhou, M., and Kan, H.: Ambient Ozone Pollution and Daily  
601 Mortality: A Nationwide Study in 272 Chinese Cities, *Environ. Health*  
602 *Perspect.*, 125, 117006, <https://doi.org/10.1289/EHP1849>, 2017.  
603
- 604 Zeng, G., Morgenstern, O., Braesicke, P., and Pyle, J. A.: Impact of  
605 stratospheric ozone recovery on tropospheric ozone and its budget, *Geophys.*  
606 *Res. Lett.*, 37, <https://doi.org/10.1029/2010gl042812>, 2010.  
607
- 608 Zeng, G., Morgenstern, O., Shiona, H., Thomas, A. J., Querel, R., and Nichol,  
609 S. E.: Attribution of recent ozone changes in the Southern Hemisphere mid-  
610 latitudes using statistical analysis and chemistry–climate model simulations,  
611 *Atmos. Chem. Phys.*, 17, 10495–10513, [https://doi.org/10.5194/acp-17-](https://doi.org/10.5194/acp-17-10495-2017)  
612 [10495-2017](https://doi.org/10.5194/acp-17-10495-2017), 2017.  
613
- 614 Zeng, L., Yang, Y., Wang, H., Wang, J., Li, J., Ren, L., Li, H., Zhou, Y., Wang,  
615 P., and Liao, H.: Intensified modulation of winter aerosol pollution in China by  
616 El Niño with short duration, *Atmos. Chem. Phys.*, 21, 10745–10761,  
617 <https://doi.org/10.5194/acp-21-10745-2021>, 2021.  
618
- 619 Zhai, S., Jacob, D. J., Brewer, J. F., Li, K., Moch, J. M., Kim, J., Lee, S., Lim,  
620 H., Lee, H. C., Kuk, S. K., Park, R. J., Jeong, J. I., Wang, X., Liu, P., Luo, G.,  
621 Yu, F., Meng, J., Martin, R. V., Travis, K. R., Hair, J. W., Anderson, B. E.,  
622 Dibb, J. E., Jimenez, J. L., Campuzano-Jost, P., Nault, B. A., Woo, J.-H., Kim,  
623 Y., Zhang, Q., and Liao, H.: Relating geostationary satellite measurements of  
624 aerosol optical depth (AOD) over East Asia to fine particulate matter (PM  
625 2.5 ): insights from the KORUS-AQ aircraft campaign and GEOS-Chem model  
626 simulations, *Atmos. Chem. Phys.*, 21, 16775–16791,  
627 <https://doi.org/10.5194/acp-21-16775-2021>, 2021.  
628
- 629 Zhao, H., Zheng, Y., Zhang, Y., Li, T., and Li, T.: Evaluating the effects of  
630 surface O<sub>3</sub> on three main food crops across China during 2015-2018.,  
631 *Environ. Pollut.*, 258, 113794–113794,  
632 <https://doi.org/10.1016/j.envpol.2019.113794>, 2020.  
633



- 634 Zhao, Z. and Wang, Y.: Influence of the West Pacific subtropical high on  
635 surface ozone daily variability in summertime over eastern China, *Atmos.*  
636 *Environ.*, 170, 197–204, <https://doi.org/10.1016/j.atmosenv.2017.09.024>,  
637 2017.  
638
- 639 Zheng, B., Gu, D., Lin, A., and Li, C.: Dynamical mechanism of the  
640 stratospheric quasi-biennial oscillation impact on the South China Sea  
641 Summer Monsoon, *Sci. China Earth Sci.*, 50, 1424–1432,  
642 <https://doi.org/10.1007/s11430-007-0075-z>, 2007.  
643
- 644 Zheng, B., Tong, D., Li, M., Liu, F., Hong, C., Geng, G., Li, H., Li, X., Peng, L.,  
645 Qi, J., Yan, L., Zhang, Y., Zhao, H., Zheng, Y., He, K., and Zhang, Q.: Trends  
646 in China's anthropogenic emissions since 2010 as the consequence of clean  
647 air actions, 18, 14095–14111, <https://doi.org/10.5194/acp-18-14095-2018>,  
648 2018.  
649
- 650 Zhou, W. and Chan, J. C.: ENSO and the South China Sea summer monsoon  
651 onset, *Int. J. Climatol.*, 27, 157–167, <https://doi.org/10.1002/joc.1380>, 2007.  
652
- 653 Zhu, J., Chen, L., Liao, H., Yang, H., Yang, Y., and Yue, X.: Enhanced PM<sub>2.5</sub>  
654 Decreases and O<sub>3</sub> Increases in China During COVID-19 Lockdown by  
655 Aerosol-Radiation Feedback, *Geophys. Res. Lett.*, 48, e2020GL090260,  
656 <https://doi.org/10.1029/2020gl090260>, 2021.  
657
- 658 Ziemke, J. R., Chandra, S., Labow, G. J., Bhartia, P. K., Froidevaux, L., and  
659 Witte, J. C.: A global climatology of tropospheric and stratospheric ozone  
660 derived from Aura OMI and MLS measurements, *Atmos. Chem. Phys.*, 11,  
661 9237–9251, <https://doi.org/10.5194/acp-11-9237-2011>, 2011.  
662  
663



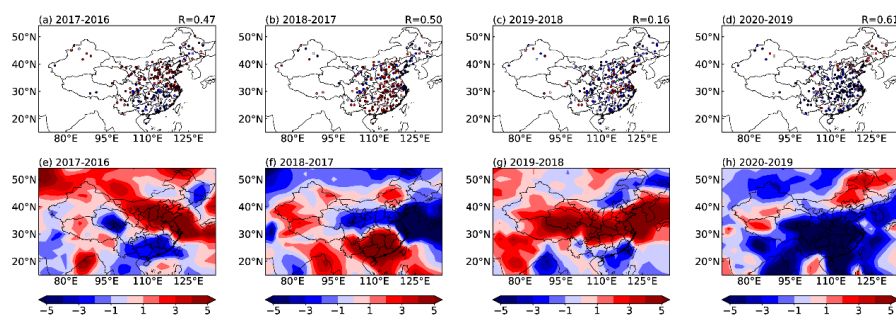
664 **Table 1.** The horizontal mass flux ( $T_g$ ) of JJA  $O_3$  from the surface to 850 hPa  
665 and the vertical mass flux ( $T_g$ ) at 850 hPa over central China ( $92.5^\circ$ – $112.5^\circ$ E,  
666  $26^\circ$ – $38^\circ$ N). The values are averaged over the selected three QBOW years  
667 (1994, 2012 and 2018) and QBOE years (1990, 1997 and 2019) and their  
668 differences (QBOW-QBOE). Positive values indicate incoming fluxes and  
669 negative values indicate outgoing fluxes.

670

	QBOW	QBOE	Difference
Horizontal mass flux			
East	1.46	2.81	-1.35
West	0.92	0.74	0.18
North	-0.06	-1.17	1.11
South	3.60	3.83	-0.23
Vertical mass flux			
Top	-5.68	-6.27	0.59

671

672



673

674

675

676

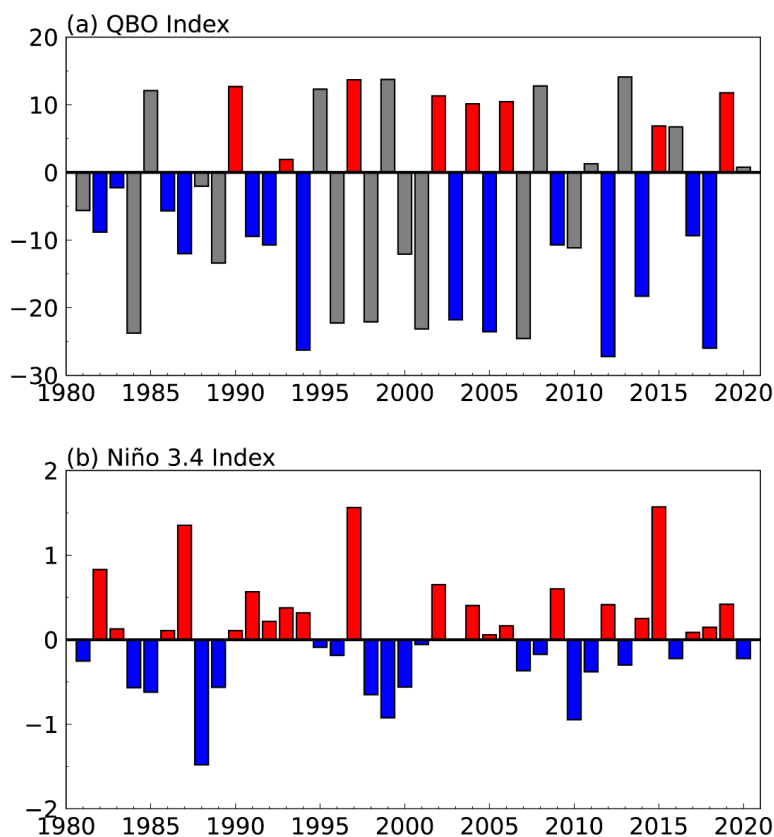
677

678

679

680

**Figure 1.** Spatial distributions of year-by-year changes in the (a-d) observed and (e-h) modeled JJA O<sub>3</sub> concentrations (ppbv) during 2016–2020. The O<sub>3</sub> observations are obtained from the China National Environmental Monitoring Centre (CNEMC). Spatial correlation coefficients between simulations and observations are shown at the top right corner of panel a-d.



681

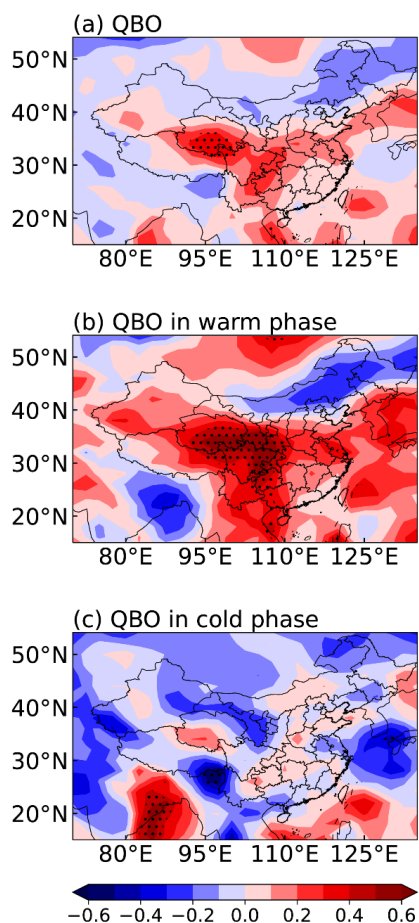
682

683 **Figure 2.** Time series of the JJA mean (a) QBO index ( $\text{m s}^{-1}$ ) and (b) Niño 3.4  
684 index ( $^{\circ}\text{C}$ ) over 1981–2020. Warm phase of SST anomalies over the eastern  
685 tropical Pacific includes 22 years (1982, 1983, 1986, 1987, 1990, 1991, 1992,  
686 1993, 1994, 1997, 2002, 2003, 2004, 2005, 2006, 2009, 2012, 2014, 2015,  
687 2017, 2018, 2019) and cold phase includes 18 years (1981, 1984, 1985,  
688 1988, 1989, 1995, 1996, 1998, 1999, 2000, 2001, 2007, 2008, 2010, 2011,  
689 2013, 2016, 2020). Colored bars in (a) indicate years with Niño 3.4 index  
690 above zero.

691

692





693

694

695

696

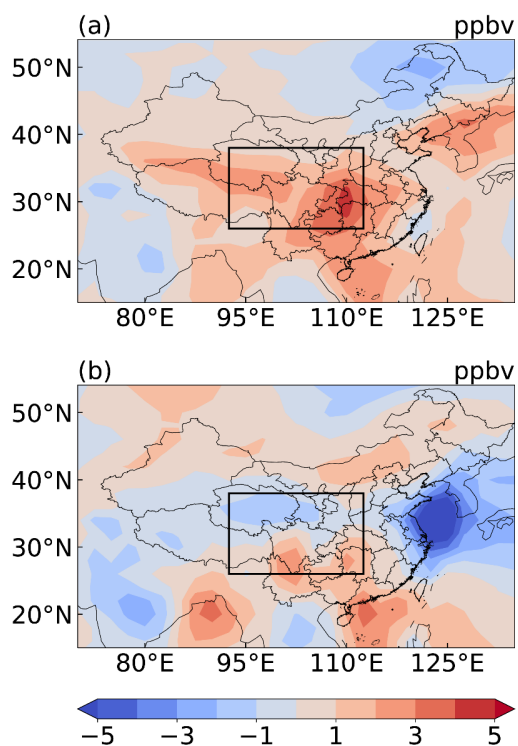
697

698

699

700

**Figure 3.** (a) Spatial distribution of the correlation coefficients between JJA near-surface O<sub>3</sub> concentrations and QBO index over 1981–2020. (b) and (c) are the same as (a), but during years having positive (22 years) and negative (18 years) SST anomalies over the eastern tropical Pacific, respectively. The stippled areas indicate statistical significance at the 90% confidence level.



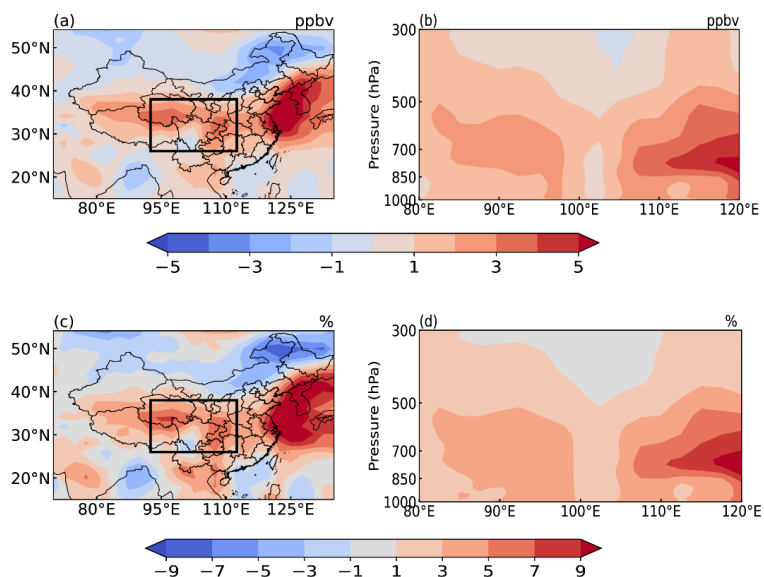
701

702 **Figure 4.** Spatial distribution of JJA surface O<sub>3</sub> concentration anomalies of (a)  
703 the selected three QBOW years (1990, 1997 and 2019), (b) the selected three  
704 QBOE years (1994, 2012 and 2018), respectively, relative to the  
705 climatological average (1981–2020).

706



707



708

709

710

711

712

713

714

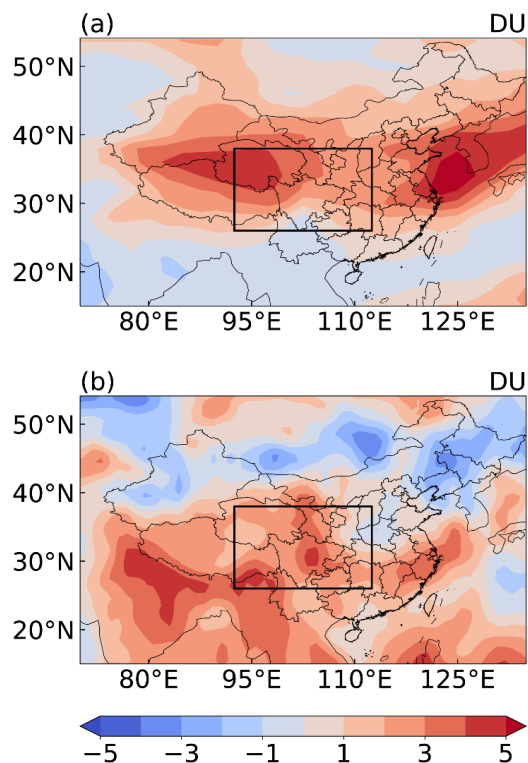
715

716

717

718

**Figure 5.** Spatial distributions of (a) absolute (ppbv) and (c) percentage (%) differences relative to the climatological mean (1981–2020) in JJA near-surface  $O_3$  concentrations between the selected three QBOW years (1990, 1997 and 2019) and QBOE years (1994, 2012 and 2018) (QBOW–QBOE). The pressure–longitude cross sections averaged over the latitudes of 26°–38°N show (b) absolute (ppbv) and (d) percentage (%) differences relative to the climatological mean in JJA  $O_3$  concentrations between the selected three QBOW years and QBOE years.

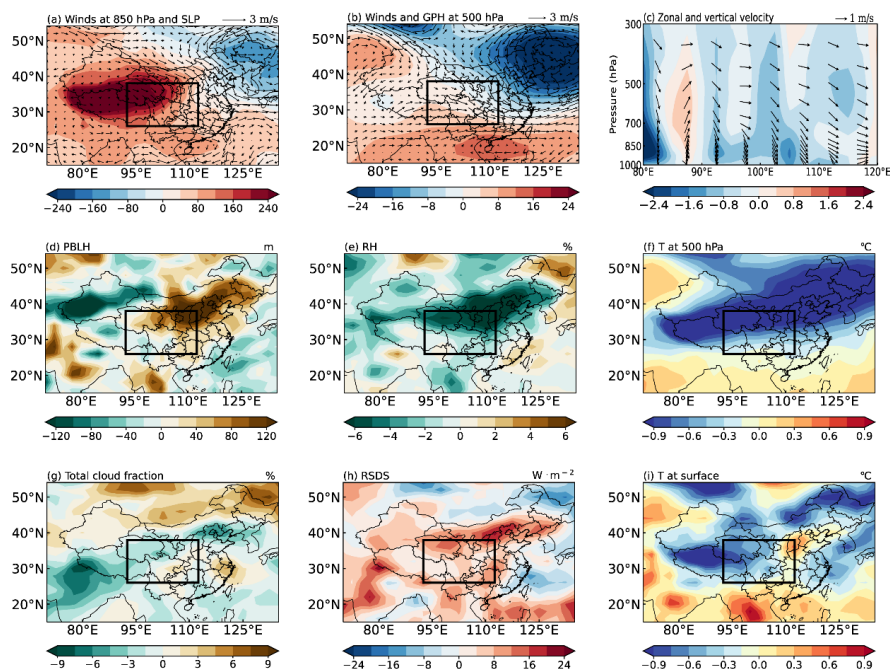


719

720 **Figure 6.** Spatial distribution of JJA tropospheric column O<sub>3</sub> (TCO, DU)  
721 difference between the selected QBOW year (2019) and QBOE year (2012,  
722 2018) based on (a) GEOS-Chem simulations and (b) Aura OMI/MLS.

723

724

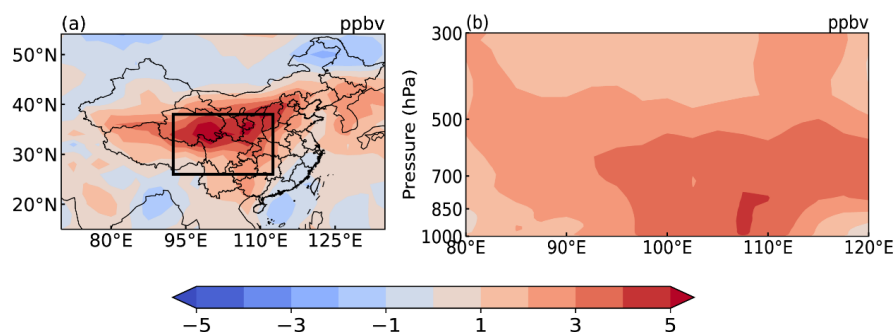


725

726 **Figure 7.** Composite differences in the spatial distribution of JJA mean (a)  
 727 wind fields ( $\text{m s}^{-1}$ , vector) at 850 hPa and sea level pressure (SLP, Pa,  
 728 contour), (b) wind fields ( $\text{m s}^{-1}$ , vector) and geopotential height (GPH, m,  
 729 contour) at 500 hPa, (d) planetary boundary layer height (PBLH, m), (e)  
 730 relative humidity (RH, %) at the surface, (f) air temperature ( $T$ ,  $^{\circ}\text{C}$ ) at 500 hPa,  
 731 (g) total cloud fraction (%), (h) downwelling shortwave radiation at the surface  
 732 (RSDS,  $\text{W m}^{-2}$ ), and (i) surface air temperature ( $T$ ,  $^{\circ}\text{C}$ ) between three QBOW  
 733 years (1990, 1997 and 2019) and QBOE years (1994, 2012 and 2018)  
 734 (QBOW–QBOE). In (c) the differences in JJA mean zonal wind ( $\text{m s}^{-1}$ , vector)  
 735 and vertical velocity (OMEGA,  $\text{Pa s}^{-1}$ , vector and contour) multiplied by a  
 736 factor of  $-100$ , averaged over  $26^{\circ}$ – $38^{\circ}\text{N}$  between three QBOW years (1990,  
 737 1997 and 2019) and QBOE years (1994, 2012 and 2018) (QBOW–QBOE).  
 738 The solid black boxes mark central China ( $92.5^{\circ}$ – $112.5^{\circ}\text{E}$ ,  $26^{\circ}$ – $38^{\circ}\text{N}$ ).

739

740



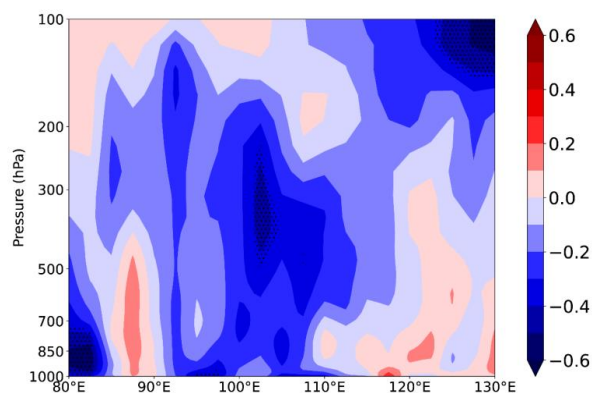
741

742 **Figure 8.** (a) Spatial distribution of differences in JJA near-surface O<sub>3</sub>  
743 concentrations (ppbv) and, (b) the pressure–longitude cross sections  
744 averaged over the latitudes of 26°–38°N of differences in JJA O<sub>3</sub>  
745 concentrations (ppbv) between three QBOW years (1990, 1997 and 2019)  
746 and QBOE years (1994, 2012 and 2018) (QBOW–QBOE) from the simulation  
747 that has the China anthropogenic emissions of O<sub>3</sub> precursors turned off  
748 (NO\_CHN). The solid black box in a marks central China.

749



750



751

752

753

754

755

**Figure 9.** Pressure-longitude distribution of the correlation coefficients between QBO index and vertical velocity (OMEGA, multiplied by a factor of  $-100$ ) in JJA averaged over  $26^{\circ}$ – $38^{\circ}$ N for years with warm SST anomaly. The stippled areas indicate statistical significance at the 90% confidence level.